ISSN: 2977-0041

Research Article

Journal of Material Sciences and Engineering Technology

Design and Characterization of Polymer-Coated MgZn Ferrite Nanoparticles: A Glycol-Thermal Approach for Biomedical Application

Mthimkhulu SS* **and Mdlalose WB**

Discipline of Physics, University of KwaZulu-Natal, Private Bag X54001, Durban 4000, South Africa

***Corresponding author**
Mthimkhulu SS, Discipline of Physics, University of KwaZulu-Natal, Private Bag X54001, Durban 4000, South Africa.

Received: October 01, 2025; **Accepted:** October 07, 2025; **Published:** October 15, 2025

ABSTRACT
This study presents the synthesis and comprehensive evaluation of $MgFe_2O_4$, $Mg_{0.5}Zn_{0.5}Fe_2O_4$, and $ZnFe_2O_4$ nanoparticles for potential use in anticancer therapy. Nanoparticles were synthesized via a glycol-thermal method and coated with chitosan (CHI) to enhance biocompatibility and stability. Structural and magnetic properties were characterized using XRD, FTIR, TEM, Mössbauer spectroscopy, and VSM. XRD confirms the formation of a single-phase cubic spinel structure, with chitosan coating increasing crystallite size and lattice parameters. FTIR confirmed chitosan coating. TEM analysis revealed spherical morphology with reduced agglomeration post-coating. Mössbauer spectroscopy showed that $MgFe_2O_4$ and Mg0.$Mg_{0.5}Zn_{0.5}Fe_2O_4$ led to ferrimagnetic behaviour, while $ZnFe_2O_4$ resulted in paramagnetism. Magnetic measurements via VSM indicated superparamagnetic behaviour in all samples, with $Mg_{0.5}Zn_{0.5}Fe_2O_4$ exhibiting the highest saturation magnetization (68.49 emu/g). Cytotoxicity assays on CaCo-2 cells demonstrated that chitosan coating significantly improved biocompatibility, particularly for $ZnFe_2O_4$, raising cell viability above 100%. These findings highlight the potential of chitosan-coated Mg-Zn ferrite nanoparticles as promising candidates for targeted drug delivery and anticancer applications.

Keywords: Nanoparticles, Spectroscopy, Magnesium, Cytotoxicity, Chitosan

Introduction

Nanoferrites have gained significant attention in biomedical applications, including drug delivery, magnetic hyperthermia, targeted therapy, and imaging resonance, due to their distinctive magnetic properties [1]. These nanoferrites, such as zinc and magnesium, have promising structural and magnetic properties in biomedical applications due to their biocompatibility, degradability, and low toxicity at concentrations less than 125µg/mL [2]. However, they have shown drawbacks. One of the major drawbacks is the cytotoxicity brought by different factors such as synthesis methods, types of materials, reaction time, and temperature. However, their potential cytotoxicity, which varies based on synthesis conditions, poses a challenge for medical use. To mitigate or eliminate these toxic effects, natural polymers such as chitosan, polyvinyl alcohol (PVA), and polyethylene glycol (PEG) are commonly employed to coat nanoferrites [3]. The polymer-coated nanoferrites are promising for targeting drug delivery and other treatments for cancer cells due to their safer delivery and reducing the side effects on healthy tissues. The incorporation of nanoferrites with polymers brought enhancement in the visibility of growing tumours and other abnormalities [4]. This surface modification enhances biocompatibility, making them safer and more effective for clinical applications. In this study, $MgFe_2O_4$, $Mg_{0.5}Zn_{0.5}Fe_2O_4$, and $ZnFe_2O_4$ nanoparticles (NPs) were synthesized and coated with chitosan (CHI) for potential applications in cancer treatment, using the glycol-thermal method. The nanoparticles were synthesized and subsequently coated with chitosan via the glycol-thermal and wet coating methods, respectively. Comprehensive characterization of the structural, morphological, and magnetic properties of the NPs was conducted using various techniques, including X-ray diffraction (XRD, MinFlex 300/600 with Cu X-ray tube), transmission electron microscopy (TEM, JEOL 1400 operated at 200 kV), Fourier-transform infrared spectroscopy (FTIR, PerkinElmer Spectrum IR Version 10.7.2),

Citation: Mthimkhulu SS, Mdlalose WB. Design and Characterization of Polymer-Coated MgZn Ferrite Nanoparticles: A Glycol-Thermal Approach for Biomedical Application. J Mat Sci Eng Technol. 2025. 3(4): 1-4. DOI: doi.org/10.61440/JMSET.2025.v3.76

Mössbauer spectroscopy, and vibrating sample magnetometer (VSM, cryogenic Ltd., UK).

Experimental

Synthesis Method

All three samples were synthesized using the same procedure. For the synthesis of $MgFe_2O_4$, magnesium chloride ($MgCl_2$) and iron (III) chloride hexahydrate ($FeCl_3 \cdot 6H_2O$) were dissolved in deionized water under continuous stirring. Sodium hydroxide was added dropwise to the solution to induce precipitation, maintaining the pH between 9 and 10. The resulting precipitate was transferred into a Büchner funnel and filtered under vacuum. Multiple washes with deionized water were performed to remove residual chlorides. The solvent was then replaced with 200 mL of ethylene glycol, chosen for its high boiling point (197 °C). The mixture was transferred to a stainless-steel pressure reactor (Watlow Series, PARR 4843) and heated at 200 °C for 6 hours. After the reaction, the product was washed again to remove ethylene glycol, followed by a final wash with ethanol. The resulting powder was dried under an infrared lamp for 24 hours, then ground and weighed using an agate mortar and pestle. $Mg_{0.5}Zn_{0.5}Fe_2O_4$, and $ZnFe_2O_4$ NPs were also synthesized following the same method described.

Coating Method

The obtained $MgFe_2O_4$, $Mg_{0.5}Zn_{0.5}Fe_2O_4$, and $ZnFe_2O_4$ NPs were coated with chitosan using a modified version of the wet chemistry method described by Mngadi et al. [5]. To prepare the chitosan solution, 1 g of chitosan was dissolved in 200 mL of acetic acid, and the pH was adjusted to 4.8 by adding sodium hydroxide. The synthesized nanoparticles 0.4 g were then dispersed in the chitosan solution and stirred for 30 minutes. The mixture was further stirred at room temperature for 18 hours using an IKA RW 20 Digital Dual-Range Mixer System. The resulting homogenous mixture was centrifuged with deionized water five times at 300 rpm for 30 minutes. After centrifugation, the sample was dried under infrared radiation for 24 hours, ground, and labeled as CHI-$MgFe_2O_4$, CHI-$Mg_{0.5}Zn_{0.5}Fe_2O_4$, and CHI-$ZnFe_2O_4$.

Results

X-ray Diffraction exhibits all the synthesized and coated NPs patterns as shown in Figure 1. All diffraction planes (hkl) (111), (220), (311), (222), (400), (422), and (440) were confirmed by the original magnetite pattern that was for a single cubic spinel structure [5]. No impurities were detected after chitosan coating. The crystallite sizes were calculated using Scherrer's equation. It was found to be decreasing after chitosan coating, except for the doped sample, which was increasing. The increase of crystallite size in the Mg0.5Zn0.5Fe2O4 sample was due to the substitution of the ionic radii of magnesium (0.65 Å) with zinc (0.83 Å), since zinc has a greater ionic radius than magnesium, which leads to lattice expansion [6]. FTIR spectra are seen in Figure 2. A broad peak around 3000-3500 cm-1 is associated with hydrogen bonding. Around 2800-3000 cm-1 and 1650-1660 cm-1, there are two stretching bands that represent the amid groups. The N-H stretching bonding peaks at 1500-1800 cm-1 are associated with chitosan, which appears on the coated samples, confirming chitosan coating. The strongest peak at 500-550 cm-1 is due to Fe-O bonding.

TEM exhibited spherical-shaped particles with an average particle distribution of 15.67 nm and 13.66 nm for as-prepared and chitosan-coated NPs, respectively. The Gaussian fit was utilized to estimate particle distribution using ImageJ software. All NPs exhibited spherical shapes, as seen in Figure 3. The chitosan-coated NPs are less agglomerated. On the doped $Mg_{0.5}Zn_{0.5}Fe_2O_4$, the bigger particles were associated with Mg^{2+}, whereas the small NPs were for Zn^{2+}. Magnesium has bigger particles due to the high synthesis temperature of 200°C, which caused them to be bigger in shape and size [7]. The decrease in particle sizes of $MgFe_2O_4$ and $ZnFe_2O_4$ after chitosan and an increase in $Mg_{0.5}Zn_{0.5}Fe_2O_4$ were observed, which affects the magnetic properties.

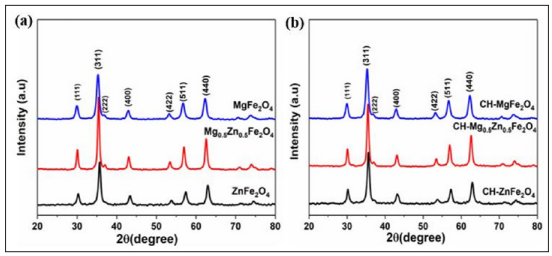

Figure 1: X-ray diffraction pattern of (a) as-prepared and (b) chitosan-coated nanoparticles.

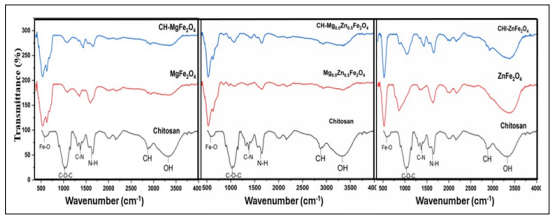

Figure 2: Fourier Transform Infrared images of as-prepared and chitosan-coated NPs.

Table 1: Crystallite size (D_{XRD}), particle size (D_{TEM}), lattice parameter (a), saturation magnetization (M_S), coercivity field (H_C) parameters

Samples	D_{XRD} (nm)±1.3	D_{TEM} (nm)±3.1	a (Å)±0.04	M_S(emu/g) ±2.46	H_C(Oe) ±0.002
$MgFe_2O_4$	13.78	15.01	8.348	62.95	10.00
CHI-$MgFe_2O_4$	12.95	13.02	8.358	64.47	13.00
$Mg_{0.5}Zn_{0.5}Fe_2O_4$	16.24	21.00	8.404	68.49	33.00
CHI-$Mg_{0.5}Zn_{0.5}Fe_2O_4$	16.76	17.02	8.399	58.81	26.00
$ZnFe_2O_4$	11.68	11.02	8.426	25.19	66.00
CHI-$ZnFe_2O_4$	11.17	10.96	8.431	27.16	69.00

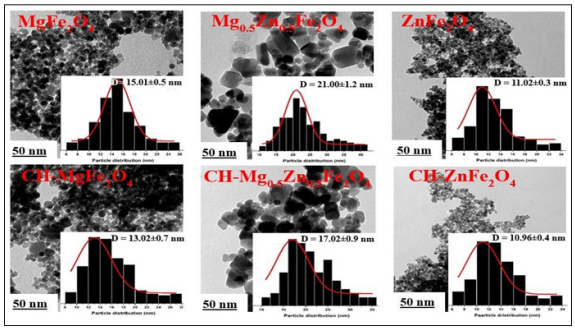

Figure 3: TEM images of as-prepared and chitosan-coated NPs

Magnetic properties are revealed by Mössbauer spectroscopy and the vibrating sample magnetometer. Mössbauer spectroscopy investigates the dominance of Fe-ions in a sample and the type of magnetization behavior [8]. The Mössbauer spectra obtained for the $MgFe_2O_4$ and $Mg_{0.5}Zn_{0.5}Fe_2O_4$ samples were successfully fitted with two sextets, indicating ferromagnetic behaviour. Based on the average of isomer shifts (IS) and hyperfine fields (Hf) for $MgFe_2O_4$ sample, Sextet A (IS = 0.31 mm/s, Hf = 296 kOe) was attributed to Fe^{2+} ions occupying tetrahedral sites, while Sextet B (IS = 0.32 mm/s, Hf = 325 kOe) corresponded to Fe^{2+} ions located on the octahedral sites [9]. A similar analysis was conducted for the $Mg_{0.5}Zn_{0.5}Fe_2O_4$ sample, where Sextet A (IS = 0.37 mm/s, Hf = 337 kOe) was attributed to Fe ions occupying the tetrahedral sites, while Sextet B (IS = 0.36 mm/s, Hf = 306 kOe) was assigned to Fe ions located at the octahedral sites. Notably, the $MgFe_2O_4$ sample exhibited a predominance of Fe ions in tetrahedral sites, whereas Fe ions were more concentrated in octahedral sites in the $Mg_{0.5}Zn_{0.5}Fe_2O_4$ sample. In contrast, the $ZnFe_2O_4$ sample displayed a spectrum fitted with two doublets, suggesting that all Fe ions were present in paramagnetic states across two distinct sites. Moreover, the magnetic properties of the nanoparticles were validated through VSM measurements, with the results presented in Table 1.

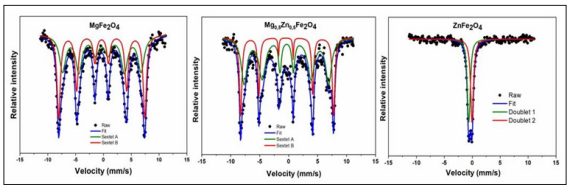

Figure 4: Mössbauer spectroscopy of nanoparticles at room temperature.

From the small average values, saturation (Ms = 52.21 emu/g) and remanent (Mr = 0.81 emu/g) magnetizations exhibited superparamagnetic behaviour in all samples, as seen in Figure 4. However, an increase in the values of Ms was observed, which is attributed to the action of chitosan as a stabilizing agent [10]. Moreover, the decrease in saturation of the $Mg_{0.5}Zn_{0.5}Fe_2O_4$ sample was due to the new non-magnetic layer added, which caused disturbance in the magnetization interaction, leading to a decrease in magnetization [10]. $MgFe_2O_4$ and $Mg_{0.5}Zn_{0.5}Fe_2O_4$ NPs have higher saturation magnetization than zinc, which was revealed by Mössbauer spectroscopy with ferromagnetic behaviour. $ZnFe_2O_4$ has a hysteresis loop of the lowest saturation magnetization (26.17 emu/g), revealing pure superparamagnetic Fe-ions, as confirmed by Mössbauer results. All synthesized and chitosan-coated nanoparticles exhibited superparamagnetic behaviour, as indicated by saturation (M_s) and remanent (M_r) magnetization values [10]. Chitosan coating stabilizes the particles, reduces agglomeration, which leads to an increase in Ms, and improves domain alignment [11]. However, $Mg_{0.5}Zn_{0.5}Fe_2O_4$ showed reduced Ms due to the presence of a non-magnetic layer disrupting magnetic interactions. $MgFe_2O_4$ and $Mg_{0.5}Zn_{0.5}Fe_2O_4$ have higher Ms than $ZnFe_2O_4$, which showed the lowest Ms and purely superparamagnetic behaviour, consistent with Mössbauer results. The superparamagnetic properties of ferrite nanoparticles make them promising for cancer treatment, though they have the potential to induce cytotoxic effects. However, additional research is needed to evaluate their toxicity on various cell lines [5]. One of the features of suitable magnetic materials for medical applications is that the particles are superparamagnetic [3]. Hence, VSM results suggest that these materials could be used in cancer treatment applications. However, they exhibit toxicity to healthy cells; as a result, the evaluation in different cell lines was performed.

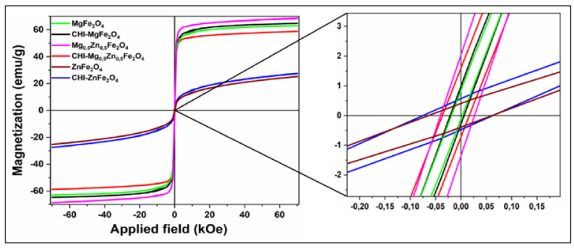

Figure 5: Hysteresis loop of as-prepared and chitosan-coated (CHI) nanoparticles measured at room temperature.

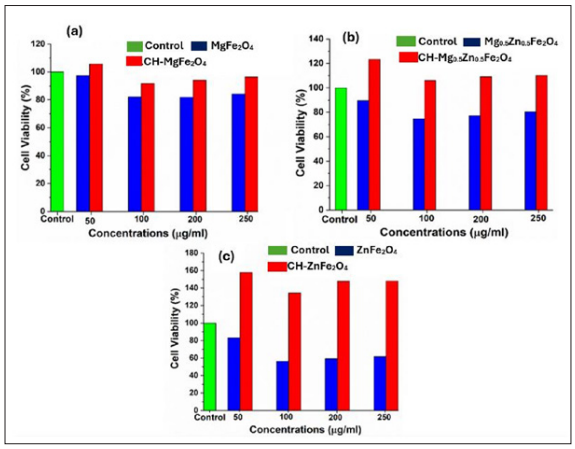

Figure 6: MTT Cell viability assay in the Human Colorectal Adenocarcinoma (CaCo-2) cell line.

A cytotoxicity study using the MTT assay on CaCo-2 cells showed that $MgFe_2O_4$ and $Mg_{0.5}Zn_{0.5}Fe_2O_4$ nanoparticles had low toxicity, maintaining over 75% cell viability, while $ZnFe_2O_4$ showed higher toxicity with viability below 60%. Chitosan-coated nanoparticles significantly improved biocompatibility, with CHI-$MgFe_2O_4$ showing over 90% viability and both CHI-$Mg_{0.5}Zn_{0.5}Fe_2O_4$ and CHI-$ZnFe_2O_4$ exceeding 100%. The chitosan coating effectively reduced nanoparticle-induced toxicity, making these nanocomposites promising for drug delivery and gene therapy applications.

Conclusion

All synthesized and chitosan-coated $MgFe_2O_4$, $Mg_{0.5}Zn_{0.5}Fe_2O_4$, and $ZnFe_2O_4$ nanoparticles exhibited a cubic spinel structure and spherical morphology, with reduced agglomeration

after chitosan coating. Magnetic characterization showed ferromagnetic behaviour for $MgFe_2O_4$ and $Mg_{0.5}Zn_{0.5}Fe_2O_4$, and paramagnetic behaviour for $ZnFe_2O_4$. All samples displayed superparamagnetic properties. Cytotoxicity studies on CaCo-2 cells revealed that uncoated nanoparticles were more toxic at higher concentrations, while chitosan-coated nanoparticles significantly improved cell viability [12]. These results highlight the potential of chitosan-coated nanoparticles for safe and effective use in gene delivery and drug nanocarrier applications.

References

1. Bucak S, Yavuztürk B, Sezer AD, Bucak S, Yavuztürk B, et al. Magnetic Nanoparticles: Synthesis, Surface Modifications and Application in Drug Delivery. Recent Advances in Novel Drug Carrier Systems. 2012.
2. Mokhosi SR, Mdlalose W, Nhlapo A, Singh M. Advances in the Synthesis and Application of Magnetic Ferrite Nanoparticles for Cancer Therapy. Pharmaceutics. 2022. 14: 937.
3. Ndlovu NL, Mdlalose WB, Ntsendwana B, Moyo T. Evaluation of Advanced Nanomaterials for Cancer Diagnosis and Treatment Multidisciplinary Digital Publishing Institute. 2024.
4. Verma R, Chauhan A, Kalia R, Batoo KM, Kumar R. Magnetic nanoferrites as an alternative for magnetic resonance imaging application. Magnetic Nanoferrites and their Composites: Environmental and Biomedical Applications. 2023. 237-256.
5. Mngadi S, Mokhosi S, Singh M, Mdlalose W. Chitosan-functionalized Mg0.5Co0.5Fe2O4 magnetic nanoparticles enhance delivery of 5-fluorouracil in vitro. Coatings. 2020. 10.
6. Abdulwahab KO, Khan MM, Jennings JR. Ferrites and ferrite-based composites for energy conversion and storage applications. Taylor and Francis Ltd. 2023.
7. M. A. Durand, The Coefficient of Thermal Expansion of Magnesium Oxide. Physics (College Park Md). 1936. 7: 297-298.
8. Choi EJ, Ahn Y, Song KC. Mössbauer study in zinc ferrite nanoparticles. J Magn Magn Mater. 2006. 301: 171-174.
9. Tunable E, lacovo A, Frigerio J, Meille S, Nakajo S. Mössbauer effect study of a polycrystalline Fe1+xCr2-xO4 spinel grown by solid-state synthesis. J Phys Conf Ser. 2022. 2164: 12067.
10. Freire TM, Dutra L, Queiroz D, Ricardo N, Barreto K, et al. Fast ultrasound assisted synthesis of chitosan-based magnetite nanocomposites as a modified electrode sensor. Carbohydr Polym. 2016. 151: 760-769.
11. Fiddaroini S, Indu K, Madaniyah L, Amalia S, Rahman M, et al. Chitosan-Coated silver nanoparticles with various floral honey bioreductors: A promising nonalcoholic hand gel sanitizer formulation. OpenNano. 2025. 21: 100228.
12. Salehi F, Behboudi H, Kavoosi G, Ardestani SK. Chitosan promotes ROS-mediated apoptosis and S phase cell cycle arrest in triple-negative breast cancer cells: evidence for intercalative interaction with genomic DNA. RSC Adv. 2017. 7: 43141-43150.